JOURNAL OF Materials CHEMISTRY

Fluence and current density dependence of silver nanocluster dimensions in ion-implanted fused silica

Marta Antonello,[a] George W. Arnold,[b] Giancarlo Battaglin,[c] Renzo Bertoncello,*[a] Elti Cattaruzza,[b] Paolo Colombo,[d] Giovanni Mattei,[b] Paolo Mazzoldi[b] and Fiorella Trivillin[a]

[a]*Unità I.N.C.M., Dipartimento di Chimica Inorganica, Metallorganica ed Analitica, via Loredan 4, 35131 Padova, Italy*
[b]*Unità I.N.F.M., Dipartimento di Fisica, Università di Padova, via Marzolo 8, 35131 Padova, Italy*
[c]*Unità I.N.F.M., Dipartimento di Chimica Fisica, Dorsoduro 2137, 30123 Venezia, Italy*
[d]*Dipartimento di Ingegneria Meccanica, Sezione Materiali, Università di Padova, via Marzolo 9, 35131 Padova, Italy*

Implantation of suitable metal ions in glass substrates leads to the formation of nanometer-size colloidal particles in a thin surface layer. The non-linear optical properties of such colloids, in particular the enhancement of optical Kerr susceptibility, suggest that the ion implantation technique may play an important role for the production of all-optical switching devices. In spite of the very large interest due to possible applications in device construction, processes governing the chemical and physical interactions between the dielectric host and the implanted metal are far from being completely understood. It is known that the formation of these particles in glasses is governed by the chemical reactivity of the substrates with the implanted ions, by the metal concentration and by its mobility. In this work, where Ag-implanted silica samples are investigated, a particular emphasis is given to the study of the dependence of the silver cluster dimensions on the ion fluence and ion current density. Silver is present in the matrix as metallic nanoclusters and the in-depth distribution of the cluster dimensions is strongly dependent on the ion current and fluence. Higher current densities favour a silver concentration increase close to the depth of maximum radiation damage. In spite of the little differences of silver total amount in the four samples, the shapes of optical absorption spectra show peculiar features strongly related to size and concentration of the silver metallic clusters.

Composite materials formed by embedding semiconductor or metal nanoclusters in glass display high non-linear properties and attract much attention as promising materials for opto-electronics, aiming to design all-optical switching devices.[1] In particular, glasses containing metal crystallites show an enhanced third-order susceptibility, whose real part is related to the intensity-dependent refractive index.[1–3] Such composites can be obtained following different routes namely, ion implantation,[4] sol–gel processes,[5] quenching and heat treatments and processes involving porous glasses.

Among these methods of synthesis, ion implantation has attracted a large interest for the possibility to pattern the materials, to overcome the doping solubility limits, and to introduce virtually any element in the glass substrate. The interaction between incident ions and substrate causes effects directly connected to radiation damage, such as mechanical stresses, density and composition modifications, and consequent mechanical, optical and chemical durability property changes. In addition to these, depending on the choice of the pair 'implanted atom–dielectric host', chemical interactions with the formation of particular compounds are possible.[6–8] Because of the interest for optoelectronic applications, most of the papers which appeared in the recent literature dealt with implantation in silica glass of metals with very weak reactivity, *i.e.* mainly copper, gold and silver: papers which review the state of the art of the research in this field appeared regularly in the literature.[7,9–11]

In spite of the large interest, processes governing the interaction between the dielectric host and the implanted metal are far from being completely understood. Our group is active in the study of the chemical interactions in silica and silicate glasses implanted with metal ions with the aim at giving a contribution to the understanding of the processes governing the interaction between the dielectric host and the implanted metal. We report in the following on results obtained for silica implanted with silver ions at a fixed energy, varying fluences and current densities in order to examine the role of these two parameters in determining the final chemical and structural state of the implanted layer. We examined samples with little variations of the implantation parameters because the mobility of silver atoms in silica can be dramatically influenced by fluence and ion current density.[12]

Experimental

Samples

Corning 7940 fused silica samples were implanted with silver at a fluence of 5×10^{16} ions cm^{-2} and current densities of 1.0 and 1.5 $\mu A\ cm^{-2}$ (LFLC and LFHC samples, respectively); other samples were implanted with silver at a fluence of 6×10^{16} ions cm^{-2} and at current densities of 1.0 and 1.5 $\mu A\ cm^{-2}$ (HFLC and HFHC samples, respectively). The meaning of the acronyms is: L = lower, H = higher, F = fluence, C = current density. The four implantations were performed at the energy of 270 keV, at room temperature and at a residual pressure of 2×10^{-4} Pa. The reproducibility of the samples has been ascertained.

Equipment

The X-ray photoelectron spectroscopy (XPS) and X-ray-excited Auger electron spectroscopy (XE–AES) measurements were achieved with a Perkin Elmer Φ 5600ci spectrometer using non-monochromatized Mg-Kα radiation (1253.6 eV). The working pressure was 10^{-7} Pa. The spectrometer was calibrated by assuming the binding energy (E_b) of the Ag $3d_{5/2}$ line at 368.2 eV with respect to the Fermi level. Depth profiles of the different elements were carried out by cycles of Ar^+

sputtering at an energy of 2.5 keV. Owing to surface charging, samples showed a shift of signal energies of 3–5 eV toward higher E_b: as internal reference for charging effects we assumed the O 1s peak of fused silica to be at 532.7 eV of E_b.[13] All over the depth profiles there is no indication of preferential sputtering induced by Ar^+ etching: the O 1s peak shape does not show any asymmetry and Si 2p E_b values always indicate the presence of stoichiometric silica. Survey scans (187.85 eV pass energy; 0.4 eV step^{-1}; 0.05 s step^{-1} dwell time) were obtained in the 0–1100 eV E_b range. Detailed scans were recorded at 58.70 eV pass energy, 0.25 eV step^{-1}, 0.1 s step^{-1} dwell time for the Si 2p, Si KLL, Ag 3d, Ag MNN, O 1s and C 1s lines. After a Shirley-type background subtraction, the raw spectra were fitted using a non-linear least-square fitting program adopting Gaussian–Lorentzian peak shapes for all the peaks. The atomic composition was evaluated using sensitivity factors as provided by Φ V5.4A software.

Transmission electron microscopy (TEM) measurements were performed at LAMEL Institute of CNR-Bologna on a Philips CM30 microscope operating at 300 kV equipped with an energy dispersive spectroscopic X-ray microanalyzer. Cross-sectional samples were prepared by mechanical prethinning followed by a low-angle milling using argon ions with energies of 5 keV. To minimize ion damage, samples were cryogenically cooled during ion milling.

Rutherford backscattering spectrometry (RBS) analyses were performed at Laboratori Nazionali INFN di Legnaro using a 2.2 MeV $^4He^+$ beam. Spectra were taken with an angle of 55° between the sample normal and the beam direction in order to enhance the profile depth scale.

UV–VIS absorption spectra in the 200–800 nm wavelength region were recorded with a CARY 5E UV–VIS–NIR dual beam spectrometer.

X-Ray diffraction (XRD) spectra were acquired with the 2θ angle ranging from 10 to 80° using Cu-Kα radiation with a wavelength $\lambda = 0.154$ nm.

Results and Discussion

RBS measurements

The concentration depth profiles of the four silver implanted samples, as determined by RBS measurements (considering the different densities of silver and silica in the $Ag + SiO_2$ system), are reported in Fig. 1. The relevant result of the four spectra is the concentration profile of silver: it is very low at the four sample surfaces and the in-depth distribution has a very peaked shape. The RBS data (summarized in Table 1) show that at the same fluence the higher current density induces a higher Ag concentration at the maximum Ag concentration depth: the silver in-depth distribution has a narrower peak shape, in accordance with literature data.[14]

These results agree well with a silver mobility dependent on

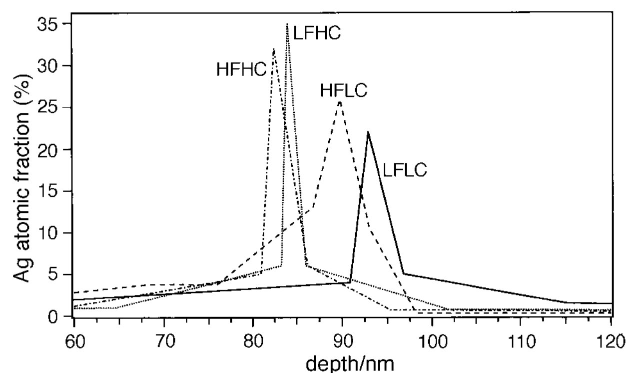

Fig. 1 Concentration depth profiles of the four different samples, as determined by RBS measurements

Table 1 Silver concentration maximum, the corresponding depth and retained dose for the four samples, as determined by RBS measurements. The TRIM calculated projected range is 130 nm

	LFLC	LFHC	HFLC	HFHC
max. Ag conc. (atom%)	22±1	35±1	26±1	32±1
depth/nm	93±3	84±3	90±3	83±3
retained dose (%)	70±3	72±3	75±3	67±3

the local radiation damage caused by the silver ion current density and fluence. Higher current densities favour the chemical behaviour of the implanted species that in the case of silver means aggregation to form larger and larger metallic clusters close to the depth of maximum radiation damage. The maximum concentration depth depends on the current density and it occurs at a depth always lower than the projected range, R_p (130 nm) calculated through the TRIM code.[15] The LC samples present the maximum concentration at depths where there is the maximum of radiation damage (93 nm), while the HC ones show their maxima at lower depths. This behaviour can be attributed to a migration of silver atoms toward the higher-damaged region of the samples,[12] followed by sample sputtering when irradiated at the higher current density.

XPS and XE–AES analyses

Silver has a very high chemical stability, so we do not expect any significative reactivity of the implanted silver atoms with the host silica matrix. XPS and XE–AES analyses establish the silver oxidation states; in particular it is possible to identify the metallic and oxidized species from the position and shape analyses of the XPS and XE–AES signals[16,17] together with the value of the 'α parameter', *i.e.* the sum of the E_b of XPS Ag $3d_{5/2}$ peak and the kinetic energy of Ag M_4NN XE–AES peak.

The analyses of the silver implanted samples do not display significant differences among the four samples: so, only the spectra of one sample (HFHC) will be discussed.

At the sample surface the Ag $3d_{5/2}$ signal has a very low intensity with an E_b value of 368.2 ± 0.1 eV. Remembering that the $3d_{5/2}$ peak components for metallic silver and silver oxides range close to an E_b value of 368.2 eV, no unambiguous evidence of the silver oxidation state can be obtained from the XPS peaks. However the Ag M_4NN XE–AES signal for the metallic and oxide species have different kinetic energy and the corresponding α parameter takes values around 726.3 ± 0.2 eV for metallic silver and ranges from 723.5 to 724.4 eV for silver oxides, as obtained from literature data[16,17] and from our standards.

In our samples the α parameter for Ag at the surface takes the value of 726.5 ± 0.2 eV. Following the depth profile we find that the α parameter does not change (within the experimental errors) indicating that silver is embedded in the silica matrix in the form of metallic species. Moreover, in the four samples, even the silver α parameter obtained by Ag $3d_{5/2}$ and Ag M_5NN (usually less used than Ag M_4NN) shows, within the experimental errors, a constant value of *ca.* 720.6 eV all over the depth profile: this indicates once more the presence of only metallic silver. In spite of this, we observe a very different behaviour of Ag $3d_{5/2}$ energy position even after the correction for the sample charging: an increase/decrease of silver concentration corresponds to a decrease/increase of the E_b of Ag $3d_{5/2}$ peak (Fig. 2): close to its concentration maximum the Ag $3d_{5/2}$ E_b value shifts down by several tenths of eV (367.2 eV for the HFHC sample, 367.9 eV for the LFLC one). This behaviour can be attributed to a silver cluster size dependent charging, *i.e.* the increase of the silver clusters dimension induces a different electrical charging of silver cluster with respect to the host silica matrix when X-ray irradiated. Even the full width

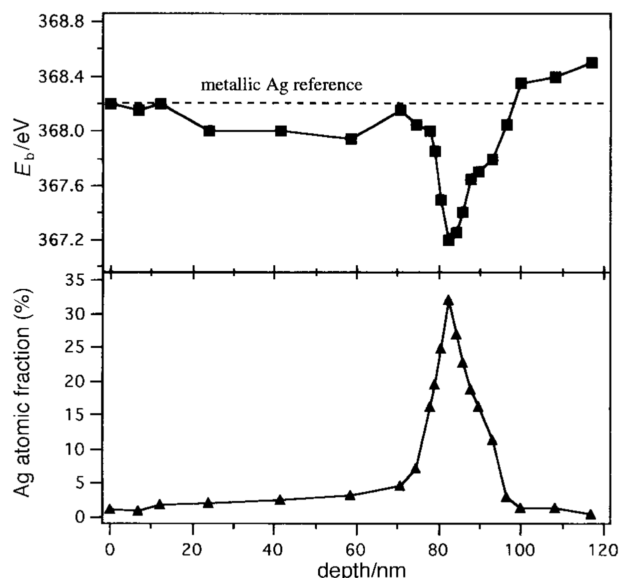

Fig. 2 XPS Ag $3d_{5/2}$ peak positions, at different depths, in the HFHC sample (■); silver depth concentration profile of silver in the same sample (▲)

at half maximum (FWHM) of the Ag $3d_{5/2}$ peak (not reported) throughout the depth profile exhibits a decrease when the Ag concentration increases, indicating a more homogeneous chemical arrangement of silver atoms (formation of very large metallic clusters).

As far as the O 1s line is concerned, there is no appreciable signal in the 529.0 eV range attributable to silver oxide along the whole profile: the value of 532.7 $\pm$ 0.1 eV for O 1s together with a value of 103.6 $\pm$ 0.1 eV for the Si 2p line observed in the XPS profile (pertinent to SiO_2) are clear indications that there is no chemical interaction between silver and the silica matrix. All these observations suggest that silver is present in the matrix as a metallic species and the Ag $3d_{5/2}$ E_b and FWHM depend on the Ag concentration. As already reported[6] the silver concentration is related to the cluster dimensions: this originates a narrowing of the silver $3d_{5/2}$ peak with increasing silver concentration. In addition, as evidenced in Fig. 2, when silver concentration increases the energy position of Ag $3d_{5/2}$ peak shifts toward E_b values lower than the reference one for bulk metallic silver.

X-Ray diffraction spectra

Usually, ion-implanted samples are not investigated by means of X-ray diffraction. This occurs even if the implanted atoms aggregate to form crystalline clusters: frequently their low concentration inside the analyzed thickness does not allow their observation. Nevertheless we have performed this investigation on our four samples because of its characteristics of easiness and of non-destructivity. The four diffraction spectra are reported in Fig. 3.

At low diffraction angles all the spectra show a large signal: this is a characteristic feature of amorphous silica. The HFHC and HFLC samples clearly show the presence of crystalline silver, whereas its characteristic diffraction peaks are hardly observable in the LFHC sample and seem to be absent in the LFLC one. Since the possibility to detect metallic nanoparticles by means of XRD measurements is related to the concentration and the mean dimension of nanocrystallites, we directly deduce from this evidence that the silver precipitation is more and more evident increasing both the ion current density and the fluence. A detailed analysis of the diffraction pattern indicates the presence of silver nanocrystals with a diameter mean value (calculated using the Debye–Scherrer formula[18]) of 12 nm for HFHC sample. In the HFLC sample the diameter mean value

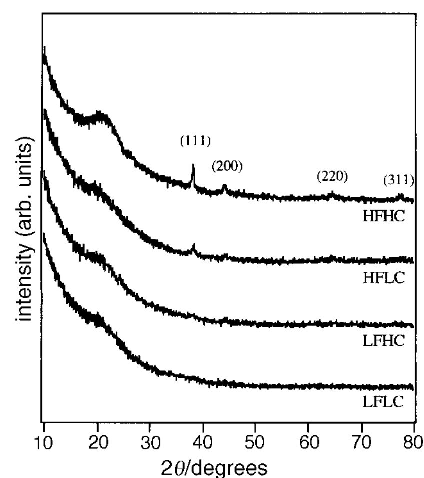

Fig. 3 XRD spectra of the four different samples. We also report the indexation of the peaks according to the silver fcc structure.

is 6 nm, while in the LFHC and LFLC ones the metallic clusters probably are too small to be detected.

TEM analyses

In the light of XRD and XPS analyses we decided to perform TEM measurements with the purpose of directly detecting the presence of Ag nanoprecipitates. We chose for this analysis the samples LFLC and HFHC, *i.e.* those giving the most different XRD spectra.

In Fig. 4 a bright field micrograph of the LFLC silver implanted sample is reported. The figure clearly shows spherical particles in the implanted region of the silica matrix.

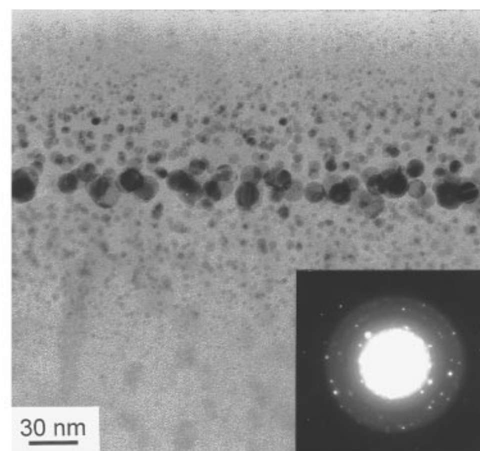

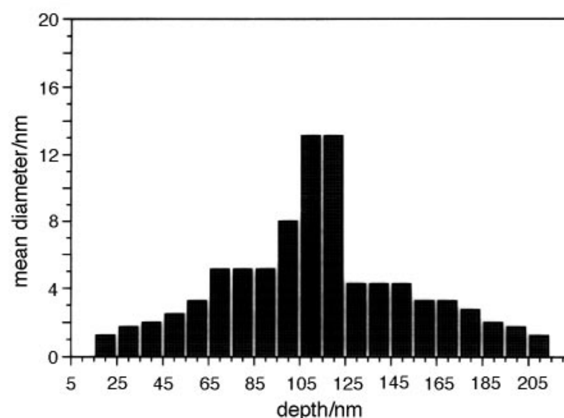

Fig. 4 Cross-section bright field TEM micrograph and in-depth distribution of the mean cluster dimensions of the LFLC sample. The inset shows the fcc (spotty) pattern of the silver nanoclusters.

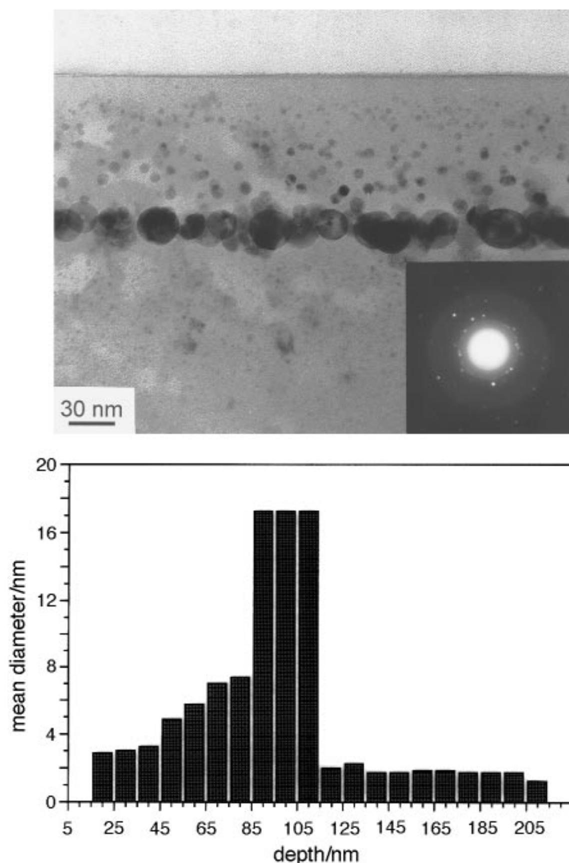

Fig. 5 Cross-section bright field TEM micrograph and in-depth distribution of the mean cluster dimensions of the HFHC sample. The inset shows the fcc (spotty) pattern of the silver nanoclusters.

Selected area diffraction (SAD) and microdiffraction with a convergent beam *ca.* 15 nm in diameter indicate that the silver clusters are crystalline. In the LFLC sample (Fig. 4) the in-depth distribution of the cluster dimension is almost symmetric with respect to the larger cluster layer (13 nm mean diameter).

In Fig. 5 the bright field micrograph of the HFHC silver implanted sample still shows spherical particles which reach a larger mean diameter (18 nm) at the maximum Ag concentration depth. The SAD indicates that the nanoparticles are crystalline. The in-depth cluster distribution in this case is no longer symmetric with respect to the larger cluster layer (Fig. 5). In particular, coming in from the surface the cluster dimensions increase up to the maximum value and then abruptly fall to a diameter close to 2 nm. The distribution of the cluster dimensions agrees with the diameter mean value obtained by XRD measurements.

TEM results are in agreement with our previous hypotheses. In particular, the diameter mean value of the nanoclusters is lower in the LFLC sample than in the HFHC one: this explains the lack of XRD peaks evidenced in the LFLC sample.

UV–VIS absorption spectra

The presence of silver nanoclusters embedded in silica originates an absorption band due to surface plasmon resonance (SPR) centered around a wavelength of 400–410 nm. Optical absorption measurements of the four different Ag-implanted silica samples are reported in Fig. 6. In the LFLC sample the high wavelength side of SPR band is slightly asymmetric. This behaviour is still more evident in the LFHC and HFLC samples and the UV–VIS spectrum of the HFHC sample clearly shows the superposition of three different bands centered at *ca.* 410, 450 and 530 nm.

The SPR phenomenon leads to sample colouring: to the eye

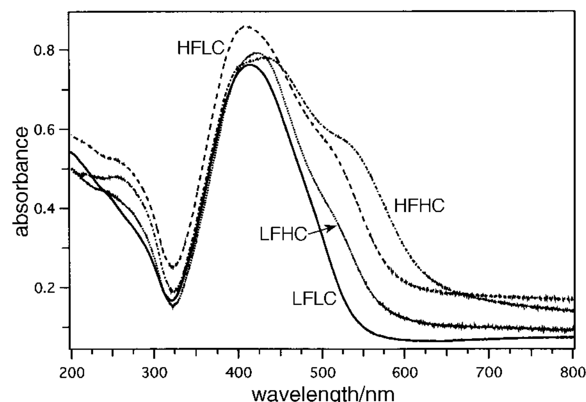

Fig. 6 UV–VIS absorption spectra of the four different samples

the LFLC sample is almost colourless, the LFHC sample is yellow and the increase of the silver fluence and current density (HFLC and HFHC samples) induce a more and more intense reddish colouring.[19] On the basis of the Mie theory[20] (adopting the electric-dipole approximation of optical absorption coefficient) the band centered at 410 nm is due to the presence of metallic silver clusters whose diameter is in the range 2–20 nm, while the bands centered at 450 and 530 nm should originate from very large metallic silver clusters whose diameter is in the range of 70–90 nm[21] (the electric-dipole approximation is no more justified when clusters diameter is larger than approximately 20 nm[22]).

TEM micrographs show that all the clusters are almost spherical and the largest ones (HFHC sample) have a diameter of *ca.* 30 nm in a very Ag-rich region. Mie theory assumes that every nanoparticle is an independent scattering point, *i.e.* the volume fraction occupied by metal cluster in the implanted layer is small. In our samples silver concentration reaches very high values, then the previous assumption should not be correct: mutual interactions among spherical nanoparticles may induce several components in absorption spectra. The bands centered at 450 and 530 nm can then be attributed to the interaction of neighbouring silver clusters as well as to the presence of high order absorption terms (*i.e.*, principally the quadrupole one).[22] This phenomenon, as shown in Fig. 6, is more manifest increasing the local silver concentration going from the LFLC up to the HFHC sample.

The UV–VIS absorption spectra evidence the same sequence of modifications that we observed in the XRD spectra: LFLC and HFHC show the greatest difference. These differences among the four samples seem induced primarily by the fluence variation, even if a small ion current density increase shows observable effects too.

All the experimental evidences can be explained considering the effects of silver radiation-enhanced diffusion (RED) during implantation: silver atoms move toward either the surface or the high-damaged region of the sample. The atoms that reach the surface are there preferentially sputtered during irradiation, while those reaching the high-damaged region aggregate to form metallic nanoclusters. In the region between the surface and the Ag maximum concentration depth a certain number of irradiation-induced defects is anyway present: these act as nucleation centers for the formation of (smaller) silver nanoprecipitates, disfavouring in this way a further Ag diffusion. In the deeper implanted layers instead the defect center density is very low. Increasing fluence and/or ion current density, the effects of silver RED increase too: more and more Ag atoms move inside the matrix inducing a higher silver concentration in a buried region of limited thickness. Here, silver aggregates to form larger and larger metallic nanoparticles. In addition, the RED induces a considerable depletion of silver in the other implanted regions. When the RED increases, this depletion

becomes more important where the density of irradiation-induced defects is lower, *i.e.* in the deeper implanted layers. Here, silver diffusion is favoured by the low concentration of nucleation centers. This argumentation is in accord with previous results,[6] even if in the case of LFHC and HFHC samples a local temperature-increase mechanism related to the variation of implantation current density may be involved.

Conclusions

Nanometer-size silver clusters may be synthesized in silica glass by ion implantation. The presence and size of such clusters depend on the fluence and ion current density: little variations of implantation parameters lead to very different situations.

XRD analyses show an increasing nanocluster concentration and mean dimension as the fluence increases. Analogous effects take place when the ion current density increases at constant fluence.

The UV–VIS optical spectra show the presence of a broad absorption band in the 300–600 nm wavelength range, with a structured shape due to the superposition of three bands centered at 410, 450 and 530 nm respectively. These bands are in agreement with the presence of a high-density region of silver clusters: the diameter of the nanoprecipitates lies in the range of 2–20 nm. The bands become more and more evident increasing the local silver concentration going from the LFLC up to the HFHC sample.

TEM analyses of the LFLC sample show that the in-depth cluster mean dimension distribution is almost symmetric with respect to the larger cluster layer, while in the HFHC sample the in-depth distribution is no more symmetric. Higher current densities seem to favour the chemical behaviour of the implanted species that in the case of silver means aggregation to form larger and larger metallic clusters, whose dimension increases close to the depth of maximum radiation damage. The maximum concentration depth depends on the current density and it occurs at a depth always lower than the calculated projected range.

Chemical investigations suggest that, within the sensitivity limits of the XPS and XE–AES analyses, silver is present in the matrix only as a metallic species; the Ag $3d_{5/2}$ XPS peak width and position depend on Ag cluster size. This means that in these systems the XPS technique is sensitive to the size of the colloids trapped in the silica matrix.

This work was partially supported by Progetto Finalizzato 'Materiali Speciali per Tecnologie Avanzate' of the CNR (Rome).

References

1 E. M. Vogel, *J. Am. Ceram. Soc.*, 1989, **72**, 719.
2 F. Hache, D. Ricard and C. Flytzanis, *J. Opt. Soc. Am. B*, 1986, **3**, 1647.
3 Y. Fainman, J. Ma and S. H. Lee, *Mater. Sci. Rep.*, 1993, **9**, 53.
4 H. Rissel and I. Ruge, in *Ion Implantation*, J. Wiley and Sons, 1986.
5 D. Kundu, I. Honma, T. Osawa and H. Komiyama, *J. Am. Ceram. Soc.*, 1994, **77**, 1110.
6 P. Mazzoldi, F. Caccavale, E. Cattaruzza, A. Boscolo–Boscoletto, R. Bertoncello, A. Glisenti, G. Battaglin and C. Gerardi, *Nucl. Instrum. Methods B*, 1992, **65**, 367.
7 G. Battaglin, *Nucl. Instrum. Methods B*, 1996, **116**, 102.
8 R. Bertoncello, F. Trivillin, E. Cattaruzza, P. Mazzoldi, G. W. Arnold, G. Battaglin and M. Catalano, *J. Appl. Phys.*, 1995, **77**, 1294.
9 P. Mazzoldi, G. W. Arnold, G. Battaglin, R. Bertoncello and F. Gonella, *Nucl. Instrum. Methods B*, 1994, **91**, 478.
10 R. F. Haglund, Jr., L. Yang, R. H. Magruder, C. H. White, R. A. Zuhr, Lena Yang, R. Dorsinville and R. R. Alfano, *Nucl. Instrum. Methods B*, 1994, **91**, 493.
11 P. Mazzoldi, G. W. Arnold, G. Battaglin, F. Gonella and R. F. Haglund, Jr., *J. Nonlinear Opt. Phys. Mater.*, 1996, **5**, 285.
12 G. W. Arnold, P. Mazzoldi, L. Tramontin, A. Boscolo-Boscoletto and G. Battaglin, *Mater. Res. Soc. Symp. Proc.*, 1993, **279**, 285.
13 M. P. Seah and G. C. Smith, in *Practical Surface Analysis*, ed. D. Briggs and M. P. Seah, Wiley, Chichester, 2nd edn., 1990, vol. 1, appendix 1, pp. 543–544.
14 N. Matsunami and H. Hosono, *Appl. Phys. Lett.*, 1993, **63**, 2050.
15 J. P. Biersack and L. G. Haggmark, *Nucl. Instrum. Methods*, 1980, **174**, 275.
16 J. F. Moulder, W. F. Stickle, P. E. Sobol and K. D. Bomben, in *Handbook of X-Ray Photoelectron Spectroscopy*, ed. J. Chastain, Perkin Elmer Corp., Eden Prairie, MN, 1992.
17 *X-Ray Photoelectron Spectroscopy Database*, version 1.0, National Institute of Standards and Technology, Gaithersburg, MD, 1989.
18 H. P. Klug and L. E. Alexander, in *X-Ray Diffraction Procedures for Polycrystalline and Amorphous Materials*, J. Wiley & Sons, New York, 1974, p. 687.
19 J. Neddersen, G. Chumanov and T. M. Cotton, *Appl. Spectrosc.*, 1992, **47**, 1959.
20 G. Mie, *Ann. Phys.*, 1908, **25**, 377.
21 G. W. Arnold and J. A. Borders, *J. Appl. Phys.* 1977, **48**, 1488.
22 U. Kreibig and M. Vollmer, in *Optical Properties of Metal Clusters*, Springer Series in Materials Science, Springer-Verlag, Berlin, Heidelberg, 1995, vol. 25.

Paper 7/05745H; *Received* 6*th August*, 1997